arXiv:2001.08716v1 [astro-ph.SR] 23 Jan 2020

Morphological Reconstruction of a Small Transient Observed by *Parker Solar Probe* on 2018 November 5

Brian E. Wood, Phillip Hess, Russell A. Howard, Guillermo Stenborg, Yi-Ming Wang[1]

[1] *Naval Research Laboratory, Space Science Division, Washington, DC 20375, USA; brian.wood@nrl.navy.mil*

ABSTRACT

On 2018 November 5, about 24 hours before the first close perihelion passage of *Parker Solar Probe* (*PSP*), a coronal mass ejection (CME) entered the field of view of the inner detector of the Wide-field Imager for Solar PRobe (WISPR) instrument onboard *PSP*, with the northward component of its trajectory carrying the leading edge of the CME off the top edge of the detector about four hours after its first appearance. We connect this event to a very small jet-like transient observed from 1 au by coronagraphs on both the *SOlar and Heliospheric Observatory* (*SOHO*) and the A component of the *Solar TErrestrial RElations Observatory* mission (*STEREO-A*). This allows us to make the first three-dimensional reconstruction of a CME structure considering both observations made very close to the Sun and images from two observatories at 1 au. The CME may be small and jet-like as viewed from 1 au, but the close-in vantage point of *PSP*/WISPR demonstrates that it is not intrinsically jet-like, but instead has a structure consistent with a flux rope morphology. Based on its appearance in the *SOHO* and *STEREO-A* images, the event belongs in the "streamer blob" class of transients, but its kinematic behavior is very unusual, with a more impulsive acceleration than previously studied blobs.
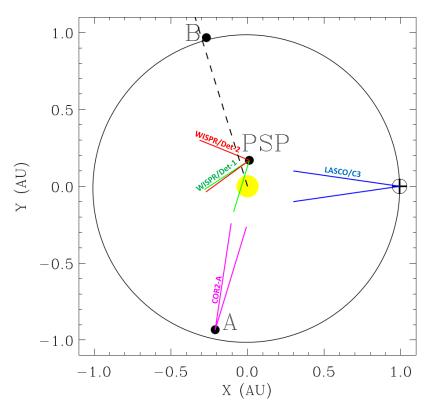
Keywords: Sun: coronal mass ejections (CMEs) — solar wind — interplanetary medium

1. INTRODUCTION

Most studies of coronal mass ejections (CMEs) naturally focus on the biggest, fastest, and brightest events, which are also the ones that are the most geoeffective when they happen to hit Earth. However, CMEs come in a wide range of sizes and speeds, with smaller, slower events being more numerous than the large, fast ones (Yashiro et al. 2004; Vourlidas et al. 2017; Wood et al. 2017). Due to their greater frequency, the smaller transients may collectively account for a significant fraction of what is generally regarded as the quiescent slow solar wind (Kilpua et al. 2009; Janvier et al. 2014).

For small transients observed in white-light (WL) images, it can be ambiguous whether "coronal mass ejection" is the best descriptive moniker. For example, using observations from the Large Angle Spectrometric COronagraph (LASCO) instrument on board the *SOlar and Heliospheric Observatory* (*SOHO*), Sheeley et al. (1997) identified a class of small jet-like transients emanating from the tops of helmet streamers, which could generically be termed "streamer disconnection events," but have been more informally called "streamer blobs" (Wang et al. 1998). These events have slow acceleration profiles that are believed to simply track the ambient slow solar wind into which they are released (Cho et al. 2018). Likewise, CMEs that have no associated solar surface activity have similarly slow acceleration profiles, and though some of these events can be large and bright, some are as small and faint as the streamer blobs (Wood et al. 2017). The distinction between streamer blobs and the slow CMEs is also blurred by morphological similarity. The stereoscopic imaging capabilities provided by the *Solar TErrestrial RElations Observatory* (*STEREO*) mission have provided evidence that streamer blobs have a flux rope (FR) structure (Sheeley et al. 2009; Rouillard et al. 2011), consistent with the most favored interpretation of CME morphology (Chen et al. 1997; Bothmer & Schwenn 1998; Thernisien et al. 2009; Vourlidas et al. 2013; Wood et al. 2017).

Even further along the spectrum from large, obvious transients toward smaller density enhancements within the solar wind are the periodic density structures identified in coronagraphic and heliospheric images (Viall et al. 2010; Viall & Vourlidas 2015). DeForest et al. (2018) find that such compact solar wind structures possess a continuum of sizes, with the streamer blobs at the large-scale end. Some of these structures might be associated with reconnection among streamer loops, others with interchange reconnection between closed loops and open flux at coronal hole boundaries, as suggested by recent numerical modeling (Higginson et al. 2017; Higginson & Lynch 2018).

Figure 1. The positions of Earth, *PSP*, *STEREO-A*, and *STEREO-B* in the ecliptic plane on 2018 November 5 (in HEE coordinates). The blue lines indicate the FOV of the LASCO/C3 coronagraph on *SOHO*, near Earth. The purple lines indicate the FOV of COR2-A on *STEREO-A*, and the green and red lines are the FOV's of WISPR's Detector 1 and Detector 2, respectively. The dashed line indicates the central trajectory of the small CME observed by LASCO, COR2-A, and WISPR on November 4-5.

The launch of *Parker Solar Probe* (*PSP*) on 2018 August 12 provides an opportunity to study small solar wind transients from a vantage point closer to the Sun, allowing a more detailed inspection of their structure. During each close perihelion passage of PSP, the plasma instruments can detect such transients in situ, and the Wide-field Imager for Solar PRobe (WISPR) instrument can provide close-up images of these events. The first perihelion passage occurred on 2018 November 6, with *PSP* reaching 35.4 $R_\odot$ from Sun-center. We here report on a small CME observed by WISPR a day earlier, which is also observed by coronagraphs on both *SOHO* and *STEREO-A*. The resulting stereoscopic imaging allows us for the first time to study CME morphology considering both multiple vantage points at 1 au and a viewpoint very close to the Sun.

2. OBSERVATIONS

The first perihelion passage of *PSP* occurred at UT 03:28 on 2018 November 6, at 35.4 $R_\odot$ from Sun-center. About 24 hours earlier, the WISPR imager on *PSP* observed the small CME that is the subject of this article, which was also detected by *SOHO*/LASCO and *STEREO-A*. Understanding these observations requires knowledge of the viewing geometry involved, which is shown in Figure 1. A heliocentric Earth ecliptic (HEE) coordinate system is used, with the x-axis pointed from the Sun toward Earth, and the z-axis pointed from the Sun toward ecliptic north. The *SOHO* spacecraft is located near Earth, specifically at the L1 Lagrangian point. The LASCO instrument on *SOHO* includes two coronagraphs, C2 and C3, observing the WL corona at Sun-center distances in the plane-of-sky of 1.5–6 $R_\odot$ and 3.7–30 $R_\odot$, respectively (Brueckner et al. 1995). The field of view (FOV) of the latter is shown explicitly in Figure 1. Also shown is the FOV of the COR2-A coronagraph on *STEREO-A*, covering 2.5–15.6 $R_\odot$ (Howard et al. 2008).

The WISPR instrument on *PSP* possesses two heliospheric imagers, Detector 1 and Detector 2, which look in the ram direction of *PSP*'s orbit around the Sun, covering elongation angles from Sun-center of $13° − 53°$ and $50° − 108°$, respectively (Vourlidas et al. 2016). These FOVs are also explicitly shown in Figure 1, although the CME in question never actually enters the Detector 2 FOV. Although *STEREO-B*'s location is indicated, observations from it are unfortunately not available, as *STEREO-B* has not been operational since late 2014.
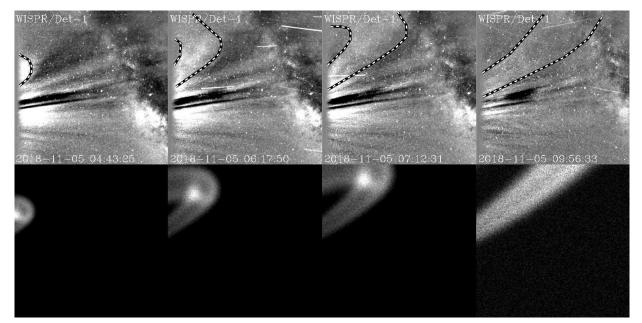
Figure 2. Images of the 2018 November 5 CME from Detector 1 of the WISPR instrument on *PSP*. The images are cropped on the bottom and right to focus attention on the region of interest. Dotted lines outline the transient. The Milky Way stretches vertically across the right side of the images. Synthetic images of the event are shown below the real images, based on the 3-D reconstruction described in Section 3. A movie version of this figure is available online.

Figure 2 shows a sequence of four WISPR Detector 1 images from UT 4:43 to UT 9:56 on 2018 November 5, with a small CME entering on the upper left side of the detector and eventually exiting off the top of the FOV. Generating such WL images requires first removing the dust-scattered F-corona contribution, which is performed as part of the WISPR data processing, analogous to what has been done for STEREO data (e.g., Stenborg & Howard 2017). This is somewhat more complicated for WISPR than for WL images from 1 au observatories, because *PSP*'s distance from the Sun is changing significantly during the observations, and therefore the F-corona background is time dependent. Removal of this background yields a WL image that includes only the K-corona contribution of interest, which is due to Thomson scattering from electrons. The K corona images are dominated by emission from the quiescent streamer structure, but we wish to focus on the emission from the transient emission. Thus, we compute an average K corona image from November 5 and then subtract this from all the images to emphasize the variable emission. We also use median filtering to suppress stellar point sources. The images in Figure 2 have been cropped on the bottom and right sides to focus attention on the location where the CME is observed.

We connect the November 5 CME observed by WISPR with a tiny transient observed by *SOHO*/LASCO on November 4–5. Figures 3 and 4 show a sequence of LASCO images from this time period. In Figure 3 the images are shown after subtracting a monthly minimum image, which preserves the appearance of the quiescent streamer structure, while in Figure 4, four C2 images are shown in a running difference format, which makes the small transient easier to see. There are actually two small transients observed by LASCO, one to the south marked by a green arrow in Figure 3, and one to the north marked by a red arrow. It is the latter that corresponds to the CME observed by WISPR. The simultaneity of the two transients suggests that they are related, both possibly resulting from a minor adjustment to the large-scale streamer structure on the west side of the Sun. In terms of their small size and clear association with the streamer structure, both events seem consistent with the "streamer blob" class of transients (Sheeley et al. 1997; Wang et al. 1998), although we will show below that the WISPR-observed event has an impulsive acceleration that is very atypical for streamer blobs. It is worth noting that despite their small size, both of these events make it into the online CDAW CME catalog (Yashiro et al. 2004, https://cdaw.gsfc.nasa.gov/CME_list), with listed start times of UT 22:12 and UT 22:36 on November 4 for the south and north events, respectively.

The origin of the event of interest is clearest in Figure 4, where the outflow begins in the middle of the FOV. There is evidence for a pinch-off region, like the events described by Sheeley & Wang (2007), leading not only to the outflowing blob but also an apparent downflow below it. This is clarified in the height-time stack plot shown in Figure 4(e), where traces of the running-difference C2 intensities at the position angle of the event are stacked. In this plot, the transient
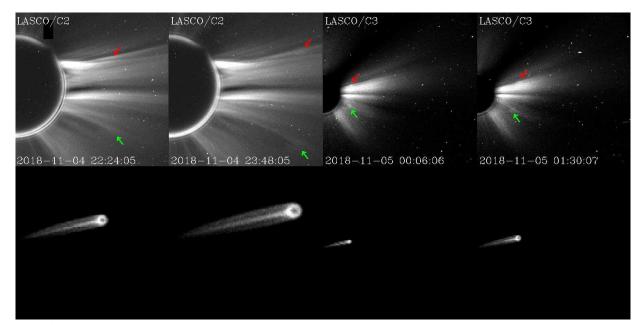
Figure 3. A sequence of images from the LASCO C2 and C3 coronagraphs on board *SOHO*, showing two little transients whose positions are marked by red and green arrows. It is the upper event that corresponds with the CME observed by WISPR. Synthetic images of this transient are shown below the real images, based on the 3-D reconstruction described in Section 3. A movie version of this figure is available online.
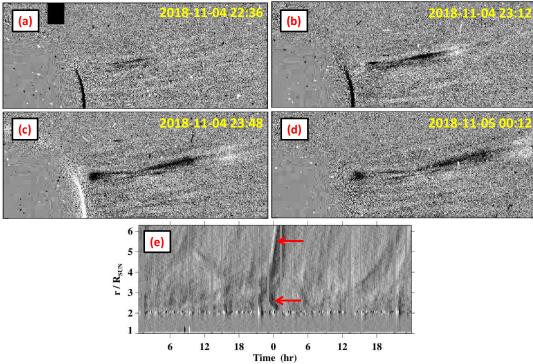

Figure 4. (a-d) A sequence of four running-difference images from the LASCO C2 coronagraph, focused on the transient observed by WISPR. (e) A height-time stack plot for the position angle of the transient, with arrows pointing towards the outflow and below it an apparent inflow.

is seen as parallel bright and dark streaks with positive slopes, indicating an outflow. A dark streak below it with a negative slope indicates the apparent downflow.

The small WISPR CME is also observed by COR2-A, as shown in Figure 5. These images are shown after the subtraction of an average COR2-A image from November 5, in order to better reveal the faint transient. The angular

Figure 5. A sequence of two images of the 2018 November 5 CME from the COR2-A coronagraph on board *STEREO-A*. Synthetic images of this transient are shown below the real images, based on the 3-D reconstruction described in Section 3. A movie version of this figure is available online.

extent of the CME in COR2-A is somewhat wider than in the LASCO images in Figures 3-4, where the CME is particularly narrow and jet-like.

It is not surprising that the CME would look much bigger in the WISPR images than in LASCO and COR2-A images from 1 au, considering how much closer *PSP* is to the event (see Figure 1). However, the most important characteristic to note about the CME's appearance is that unlike in the LASCO and COR2-A images, the CME in WISPR is not jet-like at all. Instead, the transient in WISPR looks very much like an FR structure, with two legs stretching back towards the Sun. Its appearance is dominated by one leg that ultimately stretches through the FOV from east to north, but at early times it is clear that the CME structure is not linear but bends up and then backwards, presumably curving into a second leg that is almost entirely above the FOV. It is also noteworthy that the lower leg remains visible long after the leading edge of the CME has moved out of the FOV, suggesting continued magnetic connectivity with the Sun.

Magnetic FRs can be described as tube-shaped structures permeated by a helical magnetic field, with legs that stretch back towards the Sun (Bothmer & Schwenn 1998). Evidence that FRs are at the core of all CMEs comes from both in situ plasma measurements (Lepping et al. 1990; Richardson & Cane 1996) and WL imaging (Chen et al. 1997; Thernisien et al. 2009; Vourlidas et al. 2013; Wood et al. 2017). Our observations provide further support for this interpretation, demonstrating that small CMEs that look linear and jet-like from 1 au are revealed to have an FR appearance when viewed up close. We now perform a detailed three-dimensional (3-D) reconstruction of the CME to demonstrate this more explicitly.

3. MORPHOLOGICAL RECONSTRUCTION

We reconstruct the 3-D structure of the CME assuming an intrinsic FR shape, using techniques that have been developed to interpret CME images from the *STEREO* spacecraft (Wood & Howard 2009; Wood et al. 2017). We refer the reader to this previous work for details, but in short, the shape of the inner and outer edges of a 2-D FR are defined in polar coordinates, and then the two 2-D loops are used to define a 3-D FR shape by assuming a circular cross section for the FR, bounded by the two loops. By stretching the FR in the direction perpendicular to the FR creation plane, an FR can be created with an arbitrary ellipticity. The 3-D FR is then rotated into the desired orientation in an HEE coordinate system. Adjusting the various quantities involved in the FR creation process allows experimentation with different shapes and orientations. For confronting the model FR shape with the actual images of the CME, mass is first placed onto the surface of the 3-D FR shape, but not in the interior, and then synthetic images of the resulting density cube are computed, based on calculations of the Thomson scattering within the density cube. The assessment
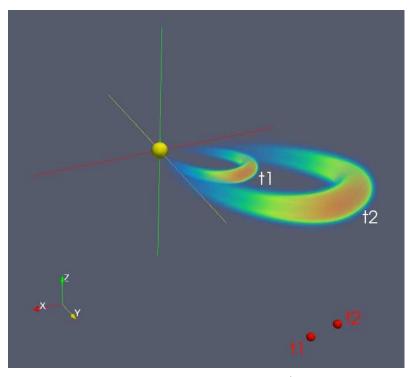
Figure 6. Reconstructed 3-D FR structure of the CME observed by *PSP*/WISPR on 2018 November 5, shown in HEE coordinates. The FR is shown at two times, t1 and t2, corresponding to UT 3:48 and UT 9:40, respectively. The red circles indicate the location of *PSP* at these two times. The size of the Sun is to scale.

of the best fit relies on subjective judgment, with the best-fit parameters discerned through trial-and-error. The shape of the CME structure is not assumed to vary at all, meaning we assume the structure expands in a self-similar fashion.

Figure 6 shows our morphological reconstruction of the CME, in an HEE coordinate system. The FR is shown at two times, UT 3:48 and UT 9:40, corresponding to the beginning and end of the movie version of Figure 2. The location of *PSP* at these two times is also indicated. The synthetic images of the CME based on this reconstruction are shown in Figures 2, 3, and 5, for comparison with the real images. The reconstruction successfully reproduces both the CME's appearance in the WISPR images (Figure 2) and the narrow, jet-like appearance in the LASCO data (Figure 3). The reconstructed FR is almost perfectly edge-on as viewed from *SOHO*'s perspective, explaining why it is so narrow in the LASCO images.

We consider the synthetic COR2-A images to be an adequate reproduction of the observations (see Figure 5), but deviations from the data are larger here. Specifically, the FR leg that is slightly higher in the COR2-A images is predicted to be brighter than observed. This is the left leg in Figure 6, which is the leg that is mostly out of the WISPR FOV in Figure 2. We suspect that improved agreement with the data could be achieved only by introducing asymmetries of some sort into our FR structure. Our parametrized FR shape is a symmetric one, with mass placed onto its surface in a symmetric fashion, increasing with distance from the Sun as r^{β} (see Figure 6), with the exponent assumed to be $\beta = 2.5$. The easiest way to improve the COR2-A appearance would be to decrease the mass in the leg that seems too bright in the synthetic COR2-A images. This would make the leg fainter in the COR2-A images, but would not meaningfully affect the WISPR or LASCO images at all, since that leg is mostly outside the WISPR FOV, and is superposed on the other, presumably brighter leg in the LASCO images.

Table 1 lists the parameters that define the shape of the FR, using the variable names from Wood et al. (2017). Briefly, λ_s and β_s are the central trajectory in HEE coordinates, with the $\lambda_s = 107°$ direction explicitly indicated in Figure 1. This longitude is very close to that of *PSP*. The FR trajectory latitude is only slightly above the ecliptic, with $\beta_s = 13°$, but the FR is so thin that this is high enough for the FR to be entirely above the ecliptic, thereby missing *PSP*. If β_s had instead been less than 5°, the CME would have likely hit the spacecraft. Although this FR passed close to the spacecraft, it was not close enough while in the WISPR FOV to resemble the kinds of FR passages that Liewer et al. (2019) modeled in their predictions of what FRs might look like in WISPR data.

The γ_s parameter indicates the tilt angle of the FR, with $\gamma_s = 0°$ corresponding to an E-W orientation parallel to the ecliptic, and $\gamma_s > 0°$ indicating an upward tilt of the west leg. With $\gamma_s = 5°$, our FR is close to being oriented perfectly

Table 1. Flux Rope Parameters

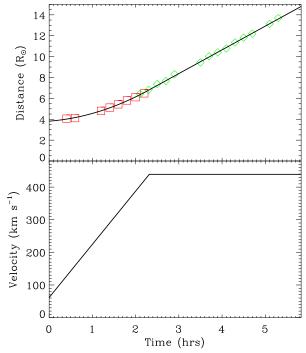| Parameter	Description	Value
λ_s (deg)	Trajectory longitude	107
β_s (deg)	Trajectory latitude	13
γ_s (deg)	Tilt angle of FR	5
FWHM_s (deg)	Angular width	43.6
Λ_s	Aspect ratio	0.039
η_s	Ellipticity of FR cross section	1.0
α_s	Shape parameter for leading edge	2.5

Figure 7. The top panel shows distance measurements for the leading edge of the 2018 November 5 CME as a function of time based on images from LASCO/C2 (red squares) and LASCO/C3 (green diamonds). The $t = 0$ point on the time axis corresponds to UT 22:00 on November 4. These data points are fitted with a simple kinematic model assuming a constant acceleration phase followed by a constant velocity phase. The solid line is the best fit, and the bottom panel shows the inferred velocity profile.

E-W. The FWHM_s parameter is the full-width-at-half-maximum angular width of the FR. Our $\mathrm{FWHM}_s = 43.6°$ value places it among the narrowest CMEs in the Wood et al. (2017) survey of 28 Earth-directed events. The aspect ratio, Λ_s, indicates the radius of the apex of the FR divided by the distance of the apex from the Sun, and so is a measure of how thin the FR is. The $\Lambda_s = 0.039$ value in Table 1 is indicative of a very thin FR, thinner than any in the Wood et al. (2017) sample. Our FR reconstruction scheme allows for the possibility of an elliptical FR channel, but we see no evidence for ellipticity, so $\eta_s = 1.0$. Finally, the α_s parameter defines the shape of the FR leading edge (see Wood et al. 2017), with higher values leading to flatter leading edges. Our rather low $\alpha_s = 2.5$ value yields a leading edge that is better described as curved rather than flat.

4. KINEMATICS

Computing the synthetic images in Figures 2, 3, and 5 requires not only the morphological reconstruction shown in Figure 6, but also a kinematic model to describe how the structure expands with time. Our kinematic measurements of the CME are based on the LASCO measurements, as LASCO has the best vantage point for tracking the leading edge of the CME. The top panel of Figure 7 shows distance measurements from the C2 and C3 coronagraphs, with measured elongation angles converted to distances assuming the CME trajectory direction found from the morphological analysis. In order to infer a velocity profile for the CME, we fit a simple two-phase kinematic model to the data, assuming a phase
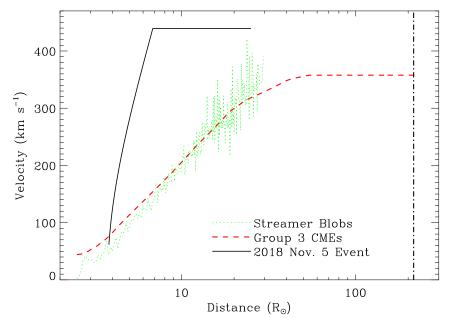
Figure 8. Velocity is plotted versus distance from Sun-center for the 2018 November 5 CME based on the kinematic model from Figure 7. This is compared with an average streamer blob kinematic profile based on measurements from Wang et al. (2000), and an average kinematic profile of Group 3 CMEs from Wood et al. (2017), which are CMEs with no associated solar surface activity. The dot-dashed line marks the 1 au distance.

of constant acceleration followed by a phase of constant velocity. In the resulting kinematic fit, the CME accelerates at a rate of 45.3 m s^{-2} for about two hours before leveling out at a final speed of 439 km s^{-1}.

Although the final speed of the CME is not particularly fast, and is comparable to slow solar wind speeds, the kinematic profile still involves a surprisingly impulsive acceleration. In order to illustrate this, in Figure 8 we compare the CME's kinematic behavior with that typically observed for streamer blobs and slow CMEs. The streamer blob profile is based on velocity-vs.-distance measurements of about 80 events from Wang et al. (2000). We place these measurements into 0.1 R$_\odot$ distance bins, and compute the average velocity within each bin, yielding the blob kinematic profile in Figure 8. For the slow CMEs, we compute the average kinematic profile of the "Group 3" CMEs in the Wood et al. (2017) sample of Earth-directed events, where "Group 3" CMEs are ones with no accompanying surface activity (e.g., flares or filament eruptions). These CMEs overlap the "streamer blowout" category of transients (Howard et al. 1985; Vourlidas et al. 2017). At this point, we should mention that inspection of images from the *Solar Dynamics Observatory* reveals no evidence of surface activity associated with the November 5 CME, but its trajectory would suggest a source 17° behind the limb as viewed from Earth, so we cannot be completely certain that no surface activity accompanies the eruption.

The streamer blobs and Group 3 CMEs have essentially identical kinematic profiles in Figure 8, involving a very slow acceleration that does not reach a terminal velocity until ~ 30 R$_\odot$. This behavior is widely assumed to be similar to that of the slow solar wind. In contrast, the 2018 November 5 transient reaches its peak speed of 439 km s^{-1} by ~ 7 R$_\odot$. The transient is very much like previously studied streamer blobs in general appearance, and is clearly associated with the quiescent streamer structure. However, its kinematics are very unusual for streamer blobs, which were first defined by Sheeley et al. (1997). More recent surveys of the blobs also do not include any events that are so impulsively accelerated (Song et al. 2009; López-Portela et al. 2018). The only clear exceptions are blob-like ejections that follow CMEs (Song et al. 2012), but there is no CME precursor for the November 5 event.

5. SUMMARY

We have studied a small transient observed by *PSP*/WISPR on 2018 November 5, which is also seen in LASCO and COR2-A coronagraphic images from *SOHO* and *STEREO-A*, respectively. Our findings are summarized as follows:

1.: Despite looking narrow and jet-like from 1 au, the WISPR images are very suggestive of an FR morphology, with a visible leg stretching back towards the Sun long after the leading edge of the transient has left the FOV.

2.: Assuming an FR shape, we perform a 3-D reconstruction of the small CME, representing the first such reconstruction considering both multiple 1 au vantage points and a viewpoint close to the Sun. Synthetic images from the reconstruction are reasonably successful at reproducing the CME appearance in the WISPR, LASCO, and COR2-A images.

3.: A kinematic fit to measurements from LASCO images implies that the CME accelerates at a rate of about 45.3 m s^{-2} to a terminal speed of 439 km s^{-1}, which it reaches at a distance of about 7 R$_\odot$ from Sun-center.

4.: The small transient looks very much like a streamer blob in the coronagraph images from 1 au, but its kinematics are unusual, with a somewhat higher speed, and a much faster acceleration. A more extensive observational study is necessary to determine whether the 2018 November 5 transient is representative of a class of streamer disconnection events that are clearly distinct from the streamer blobs studied in the past, or if the event is best described as being simply a blob with anomalously impulsive acceleration.

REFERENCES

Bothmer, V., & Schwenn, R. 1998, Ann. Geophys., 16, 1

Brueckner, G. E, Howard, R. A., Koomen, M. J., et al. 1995, Sol. Phys., 162, 357

Chen, J., Howard, R. A., Brueckner, G. E., et al. 1997, ApJ, 490, L191

Cho, I. -H., Moon, Y. -J., Nakariakov, V. M., et al. 2018, PhRvL, 121, 075101

DeForest, C. E., Howard, R. A., Velli, M., Viall, N., & Vourlidas, A. 2018, ApJ, 862, 18

Higginson, A. K., Antiochos, S. K., DeVore, C. R., Wyper, P. F., & Zurbuchen, T. H. 2017, ApJ, 840, L10

Higginson, A. K., & Lynch, B. J. 2018, ApJ, 859, 6

Howard, R. A, Moses, J. D., Vourlidas, A., et al. 2008, Space Sci. Rev., 136, 67

Howard, R. A., Sheeley, N. R., Jr., Michels, D. J., & Koomen, M. J. 1985, JGR, 90, 8173

Janvier, M., Démoulin, P., & Dasso, S. 2014, Sol. Phys., 289, 2633

Kilpua, E. K. J., Luhmann, J. G., Gosling, J., et al. 2009, Sol. Phys., 256, 327

Lepping, R. P., Jones, J. A., & Burlaga, L. F. 1990, JGR, 95, 11957

Liewer, P. C., Voulidas, A., Thernisien, A., et al. 2019, Sol. Phys., 294, 93

López-Portela, C., Panasenco, O., Blanco-Cano, X., & Stenborg, G. 2018, Sol. Phys., 293, 99

Richardson, I. G., & Cane, H. V. 1996, JGR, 101, 27521

Rouillard, A. P., Sheeley, N. R., Jr., Cooper, T. J., et al. 2011, ApJ, 734, 7

Sheeley, N. R., Jr., Lee, D. D. -H., Casto, K. P., Wang, Y. -M., & Rich, N. B. 2009, ApJ, 694, 1471

Sheeley, N. R., Jr., & Wang, Y. -M. 2007, ApJ, 655, 1142

Sheeley, N. R., Jr., Wang, Y. -M., Hawley, S. H., et al. 1997, ApJ, 484, 472

Song, H. Q., Chen, Y., Liu, K., Feng, S. W., & Xia, L. D. 2009, Sol. Phys., 258, 129

Song, H. Q., Kong, X. L., Chen, Y., et al. 2012, Sol. Phys., 276, 261

Stenborg, G., & Howard, R. A. 2017, ApJ, 839, 68

Thernisien, A., Vourlidas, A., & Howard, R. A. 2009, Sol. Phys., 256, 111

Viall, N. M., Spence, H. E., Vourlidas, A., & Howard, R. 2010, Sol. Phys., 267, 175

Viall, N. M., & Vourlidas, A. 2015, ApJ, 807, 176

Vourlidas, A., Balmaceda, L. A., Stenborg, G., & Dal Lago, A. 2017, ApJ, 833, 141

Vourlidas, A., Howard, R. A., Plunkett, S. P., et al. 2016, Space Sci. Rev., 204, 83

Vourlidas, A., Lynch, B. J., Howard, R. A., & Li, Y. 2013, Sol. Phys., 284, 179

Vourlidas, A., & Webb, D. F. 2018, ApJ, 861, 103

Wang, Y. -M., Sheeley, N. R., Jr., Socker, D. G., Howard, R. A., & Rich, N. B. 2000, JGR, 105, 25133

Wang, Y. -M., Sheeley, N. R., Jr., Walters, J. H., et al. 1998, ApJ, 498, L165

Wood, B. E., & Howard, R. A. 2009, ApJ, 702, 901

Wood, B. E., Wu, C. -C., Lepping, R. P., et al. 2017, ApJS, 229, 29

Yashiro, S., Gopalswamy, N., Michalek, G., et al. 2004, JGR, 109, A07105